MAGNETOHYDRODYNAMICS Vol. 58 (2022), No. 4, pp. 501–507
DOI: 10.22364/mhd.58.4.14

EDDY-CURRENT FLOW METER RESPONSE TO SPHERICAL NON-CONDUCTIVE INCLUSIONS TRAVELLING IN A LIQUID METAL

A. Afflard[1,2], *R. Zamansky*[1], *W. Bergez*[1], *P. Tordjeman*[1], *K. Paumel*[2]

[1] *Institut de Mécanique des Fluides de Toulouse, CNRS INPT UPS, Toulouse, France*
[2] *CEA, DES, IRESNE, DTN Cadarache, Saint Paul lez Durance, France*

In this paper, we address the problem of characterizing the size and position of a spherical non-conductive inclusion in a conductive material. The characterization is done using an Eddy-Current Flow Meter (ECFM), a device usually used to measure the flow rate of liquid metals, but which is also sensitive to the second gaseous phase. ECFM responses to the passage of inclusions in a quiescent liquid metal are computed numerically. The signal amplitude and phase variations are analyzed for inclusions of different radii and radial positions travelling in the pipe. Two parameters are introduced to characterize these variations: the maximum amplitude of the ECFM signal and its corresponding phase. It is shown that a unique relation exists between these parameters and the size and position of the inclusion. The ECFM signal thus provides enough information to determine the size and position of the inclusions by means of an inverse method. This provides valuable information for low void fraction measurement in industrial liquid metal flows.

Introduction.

In many applications, the flow of liquid metal comes with a second gaseous phase. In such two-phase flow situations, it is often essential to characterize the void fraction of the flow. This is particularly true in the context of gas leak detection in sodium/gas heat exchangers, where the bubble presence can cause safety and monitoring issues [1]. Due to the physical properties of the liquid metal, only a few measurement techniques are available for gas detection. Besides acoustic methods [2], X-ray imagery [3] or optical fibre detection [4], eddy-current methods have been proposed for the on-line measurements of the void fraction [5]. It has been observed experimentally that Eddy-Current Flow Meters (ECFM), used to monitor the flow rate of liquid metal flows, are sensitive to the passage of bubbles [6]. ECFM were subsequently considered for the detection of non-conductive inclusions travelling in a liquid metal. The ECFM usually used for void detection consist of three coaxial coils mounted side by side around the pipe [7–9]. One primary coil is supplied with an alternating current and is placed between two secondary coils that form an open electrical circuit. The secondary coils detect changes in the magnetic flux caused by the fluid flow or by the presence of any non-conductive inclusion.

For the volumetric void fraction ranging from 0.1% to 2%, Nakamoto *et al.* established correlations between the void fraction and the RMS value of the ECFM signal that depend on the flow rate [6]. However, the minimal detectable void fraction and the void measurement accuracy are not known with precision [7]. To use ECFM as low gas flow rate measurement devices, it may prove useful to study the ability of ECFM to measure the size of a single bubble in flow conditions.

Kumar *et al.* showed experimentally that under conditions of low magnetic Reynolds number $\mathrm{R_m} = \mu_0 \sigma U L$ (where μ_0 is the vacuum permeability, σ is the fluid electrical conductivity, U is the mean velocity of the fluid, and L is the diameter of the pipe) and low void fraction α, the void and velocity effects on the signal may be decoupled [7]. The

ECFM signal can therefore be decomposed into three independent components:

$$s(t) \approx s_0(t) + s_{\mathrm{u}}(t) + s_\alpha(t), \tag{1}$$

where $s_0(t)$ is the signal that accounts for the differences in the secondary coil conception, $s_{\mathrm{u}}(t)$ is the signal due to the flow, and $s_\alpha(t)$ is the signal linked to void passage. Accordingly, the study of the void effects can be performed separately from the study of the velocity effects.

With this aim, Guichou *et al.* [8] developed an analytical model that allowed computing the ECFM perturbation induced by a single inclusion. The model could predict the order of magnitude of the inclusion radius r_{b} from the amplitude of the signal induced in the ECFM. This prediction was possible only for small inclusions with large radial positions ρ. Moreover, it was assumed that the shielding parameter $S_\omega = \mu_0 \sigma \omega L^2$ verified the relation $\mathrm{R_m} \ll S_\omega \ll 1$, which constrained the analysis to low angular frequencies ω. It has been found, among others, that the maximum of the void signal amplitude varies according to:

$$\max |s_\alpha(t)| = r_{\mathrm{b}}^3 f_\omega(\rho) \mu_0 \omega \mathrm{J_e} \qquad \text{for small } r_{\mathrm{b}},\ \omega \text{ and large } \rho, \tag{2}$$

where $\mathrm{J_e}$ is the externally generated current density in the primary coil and $f_\omega(\rho)$ is a function of both ρ and ω that is characteristic to the ECFM geometry.

In this paper, we investigate numerically the sensitivity of an ECFM to void passage in the limiting case of a single spherical inclusion. Although previous research has focused on the amplitude of the signal [7, 8], both the amplitude and the phase components are analyzed here. The geometry, the numerical setup and the parameters of the study are detailed in Section 1. Results and discussions concerning the measurement of the size of an inclusion from the ECFM signal are presented in Section 2. Conclusions and further directions are given in Section 3.

1. Numerical simulations.

The ECFM response to the crossing of a single inclusion is simulated using the COMSOL Multiphysics 6.0 solver. The simulations are conducted with the liquid metal GaInSn alloy of electrical conductivity $\sigma = 3.46 \times 10^6\,\mathrm{S/m}$ in a pipe of diameter 26 mm (Fig. 1). A primary copper coil is supplied with an alternating current $i_p(t) = I_p \sin(\omega t)$ oscillating at the angular frequency $\omega = 2\pi f$. As depicted in Fig. 1, two secondary coils surround the liquid metal and form a single open circuit with zero current. The winding wire diameter is 0.28 mm. The coils are winded with multiple layers and a gap of 1 mm is left between the coils. Further specifications are provided in Table 1.

We consider a spherical inclusion moving rectilinearly in the pipe. The geometrical configuration is described by the radius of the inclusion r_{b}, its distance from the pipe axis ρ and its axial position z (Fig. 1). Displacement currents are negligible and the inclusion movement is considered slow enough to be modelled as a quasistatic process [7, 8]. The finite element method is used to solve the time-harmonic Ampère's law for the magnetic vector potential $\mathbf{A}$:

$$j\omega\sigma\mathbf{A} + \nabla \times \left(\mu_0^{-1} \nabla \times \mathbf{A}\right) - \sigma \mathbf{v} \times (\nabla \times \mathbf{A}) = \mathbf{J_e}. \tag{3}$$

Table 1. Characteristics of the ECFM coils (winding, current and dimensions).

Primary coil	63 turns × 4 layers	$I_p = 0.2\,\mathrm{A}$	19.6 mm × 1.2 mm
Secondary coils	35 turns × 4 layers	$I_s = 0\,\mathrm{A}$	11.2 mm × 1.2 mm

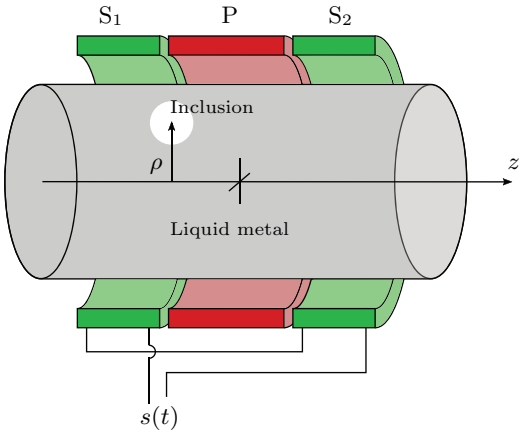

Fig. 1. Rectilinear motion of a non-conducting spherical inclusion in a liquid metal. 'P' denotes the primary coil. The inclusion travels through the ECFM along the z-direction and induces a signal $s(t)$ in the secondary coils 'S_1' and 'S_2'. The radial position of the inclusion is given by ρ.

The externally generated current density $\mathbf{J_e}$ oscillates at the angular frequency ω in the primary coil and is set to zero elsewhere. Since there are no material interface in the ECFM vicinity that imposes boundary conditions for the vector potential $\mathbf{A}$, the computational domain is extended outward until the magnetic potential tends to zero.

To focus on the effects of the rectilinear translation of an inclusion on the ECFM signal, velocity effects are removed by setting the fluid at rest in the pipe, i.e. $\mathbf{v} = \mathbf{0}$. In addition, the two secondary coils are numerically identical, so the only non-zero component of the ECFM signal in Eq. (1) is the void contribution.

The ECFM signal $s(t) = s_1(t) - s_2(t)$ is the difference between the electromotive force (emf) of the two secondary coils. This difference has zero value as long as the inclusion does not encounter the current density that is induced by the primary coil in the fluid. When the inclusion passes through the ECFM, the time-harmonic signal is subject to both amplitude and phase modulations. The time scale of these modulations is much larger than that of the current oscillation. This signal can be written using both the amplitude/phase (S, ϕ) components or the in-phase/quadrature $(s_\parallel, s_\perp)$ components:

$$s(t) = S(t)\sin\left[\,\omega t + \phi(t)\,\right] = s_\parallel(t)\sin(\omega t) + s_\perp(t)\cos(\omega t). \tag{4}$$

These modulations are computed for different radii and radial positions of the inclusion as well as for different current frequencies f. Static simulations were realized at different axial positions $z(t)$ along the inclusion trajectory and were used to reconstruct the signal as a function of z. The range of parameters studied is summarized in Table 2. Mesh convergence is assessed for all cases using the amplitude/phase components of the ECFM signal as convergence criteria and is achieved for a computational domain of 10^6 cells.

Table 2. Parameters for numerical simulations.

Parameter	Inclusion radius r_b	Radial position ρ	Frequency f
Range	1 – 3.5 mm	1 – 9 mm	500 – 9000 Hz

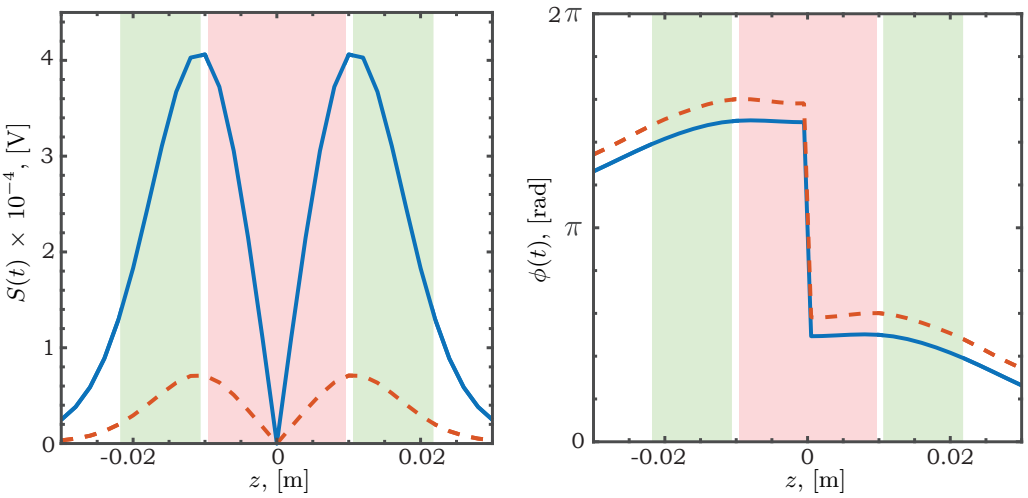

Fig. 2. Amplitude $S(t)$ and phase $\phi(t)$ of the ECFM response to the passage of an inclusion at $f = 1000$ Hz. The colored background represents the primary coil and the adjacent secondary coils surrounding the liquid; (—) $r_\mathrm{b} = 3$ mm, $\rho = 4$ mm and (----) $r_\mathrm{b} = 1$ mm, $\rho = 9$ mm.

2. Results and discussion.

The evolution of the amplitude $S(t)$ and phase $\phi(t)$ of the ECFM signal throughout an inclusion trajectory is displayed in Fig. 2. The amplitude signals present two maxima when the inclusion is located between the primary and one of the secondary coils (Fig. 2). Due to the symmetry of the problem, the amplitude signals go to zero when the inclusion is exactly in the middle of the primary coil. Regarding the phase signals, the variation indicates that the induced currents of different amplitudes and phases are disturbed by the inclusion during its passage. The phase gap of 180° observed at $z = 0$ is best captured when the signal is plotted in the in-phase/quadrature plane: it results from the signal $s_1(t) - s_2(t)$ changing sign. This is illustrated in Fig. 3, where the signals from two distinct configurations are displayed for a small inclusion far from the pipe axis ($r_\mathrm{b} = 1$ mm, $\rho = 9$ mm) and for a large inclusion near the pipe axis ($r_\mathrm{b} = 3$ mm, $\rho = 1$ mm). Although these two inclusions produce exactly the same amplitude signal, their phase components are different. This is graphically noticeable by the different tilt angles of the signal in the in-phase/quadrature $(s_\parallel, s_\perp)$ plane. In the same way, one could find inclusions that produce the same exact phase signal with a different amplitude component. It results from this observation that the volume of the inclusion cannot be deduced from the analysis of the amplitude or phase alone [8]. However, the use of both the amplitude and the phase could help to distinguish them.

With this aim, we first characterized the signal induced by the passage of one inclusion by defining two parameters: the maximum amplitude S_max and the phase ϕ_max when S_max is reached. Since the amplitude has two peaks, any of the two corresponding phases can be picked. Both parameters depend on the geometrical parameters r_b and ρ as well as on the current frequency f. To study how the size and position of an inclusion affect the signal, the values of S_max and ϕ_max were computed for a set of 54 numerical simulations. These were performed at $f = 1000$ Hz for $r_\mathrm{b} \in [1.0, 3.5]$ mm with a step of 0.5 mm and $\rho \in [1, 9]$ mm with a step of 1 mm. The resulting data are interpolated as a function of the radius r_b and radial position ρ of the inclusion (Fig. 4).

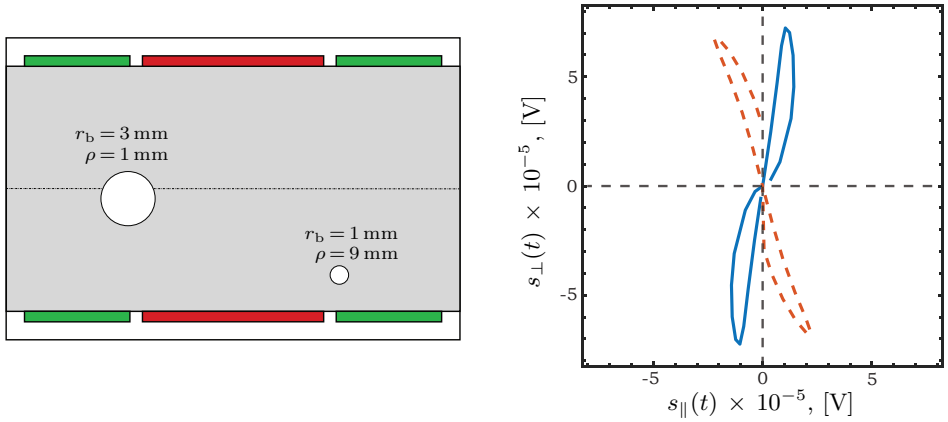

Fig. 3. Geometry of two configurations inducing an identical amplitude response and the corresponding responses of the ECFM in the phase/quadrature plane at $f = 1000$ Hz. (—) $r_b = 3$ mm, $\rho = 1$ mm and (----) $r_b = 1$ mm, $\rho = 9$ mm.

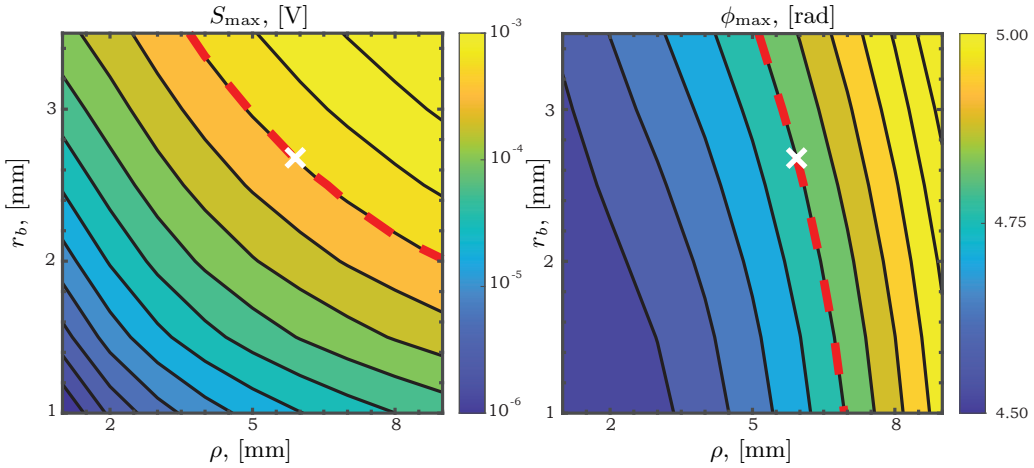

Fig. 4. The maximum amplitude S_{max} and the corresponding phase ϕ_{max} of the ECFM response for the investigated set of geometrical parameters ($f = 1000$ Hz). Dashed lines mark the arbitrarily chosen $S_{max} = 6.1 \times 10^{-4}$ V and $\phi_{max} = 4.82$ rad isovalues, respectively. The cross marks the intersection of these isolines.

In Fig. 4, it appears that the numerical value of S_{max} constrains the possible values of r_b to an entire isoline in the (r_b, ρ) plane. Besides, the information on ϕ_{max} also constrains the possible values of r_b but to a different isoline in the (r_b, ρ) plane. A single point, resulting from the intersection of the S_{max} and ϕ_{max} isolines gives not only the size but also the radial position of the inclusion. This method, similar to that of Nguyen *et al.* for surface defects [10], allows the volume and position measurement of a single inclusion as long as these isolines are not parallel. As an example, the arbitrarily chosen $S_{max} = 6.1 \times 10^{-4}$ V and $\phi_{max} = 4.82$ rad isolines and their intersection are displayed in Fig. 4.

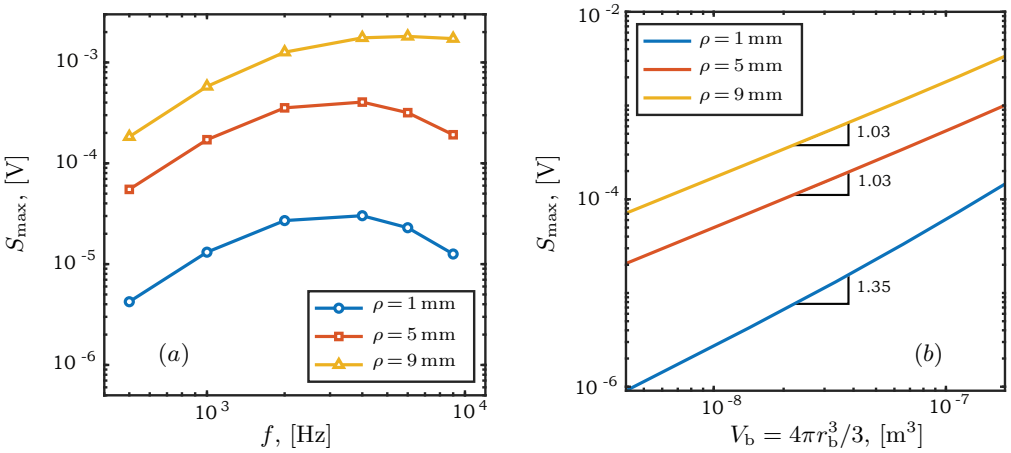

Fig. 5. (*a*) Dependence of $S_{\max}$ on the frequency of the current in the primary coil for a single inclusion of radius $r_b = 2$ mm. Three radial positions are depicted. (*b*) Dependence of $S_{\max}$ on the inclusion volume at $f = 1000$ Hz. Three radial positions are depicted. For each radial position, the slope indicates the exponent in the power law $S_{max} \propto V_b^n$. Eq. (2) corresponds to $n \approx 1$.

These results open the way for an experimental procedure of void measurement in a bubbly flow. From the experimentally measured signal $s(t)$, we isolate the successive values of $S_{\max}$ and $\phi_{\max}$ [5]. The corresponding value of r_b and ρ for each bubble is then obtained from a chart similar to that of Fig. 4. This chart might be obtained either from model experiments or from numerical simulations with an identical ECFM.

In order to know the best conditions to carry out these experiments, the previous numerical study was performed at multiple frequencies (Table 2). Although the method of the intersection of isolines is equally applicable from 500 to 9000 Hz, we focus here on the influence of f on $S_{\max}$. Experimentally, the highest value of $S_{\max}$ is of special interest since it provides the highest sensitivity to void passage and possibly the highest signal-to-noise ratio in flow conditions [6]. Fig. 5*a* illustrates this dependence in the case of inclusions of radius $r_b = 2$ mm for three different radial positions. It is possible to delimit a frequency range, where the sensitivity is relatively high for all inclusions, which is around 4000 Hz in Fig. 5*a*. The skin effect can make vary the frequency at which the amplitude reaches a maximum when changes are made on the diameter of the pipe or on the conductivity of the liquid (and by extension, its temperature). The optimal frequency range is, therefore, highly dependent on the experimental setup and its application.

As shown by Guichou *et al.* [8], the value of $S_{\max}$ evolves linearly with the inclusion volume for large radial positions ρ and for small current frequencies f. This is also observed in our simulations, and Eq. (2) is valid for all inclusion radii and all frequencies investigated. However, for inclusions close to the pipe axis, where the current density goes to zero, Eq. (2) fails, as demonstrated in Fig. 5*b*.

3. Conclusions.

The present study examines the ability of an Eddy-Current Flow Meter to characterize the volume and position of a single non-conductive inclusion in a pipe filled with a conductive fluid. The response of the ECFM to void passage is investigated numerically using COMSOL Multiphysics. It is done by simulating the signal induced by single inclusions of different radii and radial positions. The results show that the amplitude of

the ECFM signal alone is not enough to determine the size or position of the inclusion. This issue is resolved by analyzing the phase modulation. To this end, two parameters $S_{\max}$ and $\phi_{\max}$ were chosen to describe the entire ECFM signal. It was demonstrated in a particular range of parameters that a unique pair of $(S_{\max}, \phi_{\max})$ values is associated with a unique pair of (r_{b}, ρ) geometrical parameters. This result is presently limited to single spherical inclusions moving rectilinearly without flow perturbations. In these conditions, an experimental procedure is proposed to infer the size and radial position of successive inclusions from the ECFM signal generated.

These numerical simulations provide valuable information to study the case of bubble clouds in liquid metal flows. Further experimental work is required to validate these results in both static and flow configurations.

References

[1] M. Cavaro, C. Payan and J.P. Jeannot. Towards the characterization of the bubble presence in liquid sodium of sodium cooled fast reactors. In: *Proc. the 3rd International Conference ANIMMA*, (2013).

[2] A. Andruszkiewicz, K. Eckert, S. Eckert and S. Odenbach. Gas bubble detection in liquid metals by means of the ultrasound transit-time-technique. *The European Physical Journal Special Topics*, vol. 220 (2013).

[3] O. Keplinger, N. Shevchenko and S. Eckert. Experimental investigation of bubble breakup in bubble chains rising in a liquid metal. *International Journal of Multiphase Flow*, vol. 116 (2019).

[4] C. Corazza, K. Rosseel, W. Leysen, K. Gladinez, A. Marino, J. Lim and A. Aerts. Optical fibre void fraction detection for liquid metal fast neutron reactors. *Experimental Thermal and Fluid Science*, vol. 113 (2020).

[5] T. Gundrum, P. Buttner, B. Dekdouk, A. Peyton, T. Wondrak, V. Galindo and S. Eckert. Contactless inductive bubble detection in a liquid metal flow. *Sensors*, vol. 16 (2016).

[6] K. Nakamoto, S. Tamura, K. Ishii, H. Kuwahara, N. Ohmiya and T. Muramatsu. Application of an eddy-current type flowmeter to void detection at the LMFBR core exit. *Nuclear Engineering and Design*, vol. 82 (1984).

[7] M. Kumar, W. Bergez, P. Tordjeman, R. Arinero and K. Paumel. Magnetic flux distortion in two-phase liquid metal flow: Model experiment. *Journal of Applied Physics*, vol. 119 (2016).

[8] R. Guichou, H. Ayroles, R. Zamansky, W. Bergez, P. Tordjeman and K. Paumel. Perturbation of eddy-currents by one inclusion in liquid metal. *Journal of Applied Physics*, vol. 125 (2019).

[9] R. Guichou, P. Tordjeman, R. Zamansky, W. Bergez and K. Paumel. Experimental study of bubble detection in liquid metal. *Magnetohydrodynamics*, vol. 53 (2017), no. 4, pp 667–676; DOI: 10.22364/mhd.53.4.8

[10] Q. Nguyen, L. Philipp, D. Lynch and A. Pardini. Steam tube defect characterization using eddy current Z-parameters. *Research in Nondestructive Evaluation*, vol. 10 (1998).

Received 22.09.2022